Biochimica et Biophysica Acta 1864 (2017) 267–279

Contents lists available at ScienceDirect

Biochimica et Biophysica Acta

journal homepage: www.elsevier.com/locate/bbamcr

Electric field as a potential directional cue in homing of bone marrow-derived mesenchymal stem cells to cutaneous wounds

Eliza Zimolag [a,*], Julia Borowczyk-Michalowska [a], Sylwia Kedracka-Krok [b,c], Bozena Skupien-Rabian [b], Elzbieta Karnas [a], Slawomir Lasota [a], Jolanta Sroka [a], Justyna Drukala [a], Zbigniew Madeja [a,*]

[a] Department of Cell Biology, Faculty of Biochemistry, Biophysics and Biotechnology, Jagiellonian University, Gronostajowa 7, 30-387 Krakow, Poland
[b] Department of Physical Biochemistry, Faculty of Biochemistry, Biophysics and Biotechnology, Jagiellonian University, Gronostajowa 7, 30-387 Krakow, Poland
[c] Malopolska Centre of Biotechnology, Jagiellonian University, Gronostajowa 7a, 30–387 Krakow, Poland

ARTICLE INFO

Article history:
Received 19 September 2016
Received in revised form 10 November 2016
Accepted 13 November 2016
Available online 15 November 2016

Keywords:
Electrotaxis
Galvanotaxis
Electric field
Mesenchymal stem cells
Macrophages
Wound healing

ABSTRACT

Bone marrow-derived cells are thought to participate and enhance the healing process contributing to skin cells or releasing regulatory cytokines. Directional cell migration in a weak direct current electric field (DC-EF), known as electrotaxis, may be a way of cell recruitment to the wound site. Here we examined the influence of electric field on bone marrow adherent cells (BMACs) and its potential role as a factor attracting mesenchymal stem cells to cutaneous wounds. We observed that in an external EF, BMAC movement was accelerated and highly directed with distinction of two cell populations migrating toward opposite poles: mesenchymal stem cells migrated toward the cathode, whereas macrophages toward the anode. Analysis of intracellular pathways revealed that macrophage electrotaxis mostly depended on Rho family small GTPases and calcium ions, but interruption of PI3K and Arp2/3 had the most pronounced effect on electrotaxis of MSCs. However, in all cases we observed only a partial decrease in directionality of cell movement after inhibition of certain proteins. Additionally, although we noticed the accumulation of EGFR at the cathodal side of MSCs, it was not involved in electrotaxis. Moreover, the cell reaction to EF was very dynamic with first symptoms occurring within <1 min. In conclusion, the physiological DC-EF may act as a factor positioning bone marrow cells within a wound bed and the opposite direction of MSC and macrophage movement did not result either from utilizing different signalling or redistribution of investigated cell surface receptors.

1. Introduction

Cutaneous wound healing is a multistage process that employs many types of cells, including skin cells, inflammatory cells and endothelial cells [1]. The appropriate coordination of cell migration and release of cytokines or growth factors are necessary to orchestrate this process. However, in the case of extensive and deep skin injuries, the resident progenitor cells are unable to reconstitute a fully functional tissue and may be supported by cells that are primarily absent at the wound site, thus recruited from distant niches. Mounting evidence suggests that bone marrow-derived cells, including mesenchymal stem cells (BM-MSC) may be attracted to the skin lesion [2–5]. BM-MSC, also referred to as stromal progenitor cells, are self-renewing and expandable stem cells that were found to differentiate into adipocytes, osteoblasts and chondrocytes [6]. Recently, it was shown that BM-MSC play an active role in the healing process contributing to different types of skin cells, i.e. keratinocytes and fibroblasts [2,4]. Moreover, data indicate that BM-MSC also enhance healing by producing and releasing proangiogenic factors such as VEGF and angiopoietin-1 (Ang-1) or extracellular matrix proteins, i.e. collagen III [4].

Cells participating in wound healing have to be guided specifically to the site of action in order to perform their functions. Cell migration through an increasing gradient of soluble chemoattractant created in the healing tissue is a common way of cell recruitment to the wound site. However, cells may also respond by directed migration to other factors such as adhesion site gradient, matrix topography or matrix stiffness [7]. Moreover, one of the first directional cues that appears in the skin immediately after wounding is a DC-EF. A weak DC-EF is created as a result of local transepithelial potential collapse at the breached epithelium. This gives rise to a steady voltage gradient of 40–200 mV/mm directed toward the wound edge and parallel to the epithelial layer with the wound negative with respect to intact tissue [8–10]. DC-EF lasts during healing and may guide cell migration by a process known as

Abbreviations: A-BMAC, anode-migrating bone marrow adherent cells; BMAC, bone marrow adherent cells; C-BMAC, cathode-migrating bone marrow adherent cells; DC-EF, direct current electric field; MSC, mesenchymal stem cells.

* Corresponding authors.
E-mail addresses: eliza.zimolag@uj.edu.pl (E. Zimolag), z.madeja@uj.edu.pl (Z. Madeja).

http://dx.doi.org/10.1016/j.bbamcr.2016.11.011

electrotaxis or galvanotaxis. It is well documented that endogenous EFs guide fibroblasts and keratinocytes and thus accelerate the wound healing process. However, many other types of cells were shown to respond to physiological levels of EF with directed migration toward one of the electrodes, mostly to the cathode.

Although the process of electrotaxis was firstly described in the XIX century, the mechanism of electric field detection by cells is still poorly understood. One hypothesis proposed by Jaffe and then Poo and McLaughlin, assumes that the electrostatic or electroosmotic forces redistribute charged components of the cell membrane including receptors of chemoattractants, increasing their density at one site of the cell [11–13]. As a result signal propagation within a cell polarizes and leads to directional cell migration in EF. Over the last 20 years a number of membrane receptors such as epidermal growth factor receptor (EGFR), concanavalin A receptor (ConA), sodium-hydrogen exchanger 3 (pNHE3), N-methyl-D-aspartate receptor (NMDAR), acetylocholine receptor (AchR) or integrins were shown to be redistributed under EF influence and involved in cell electrotaxis [14–21]. Moreover, several downstream signalling mechanisms, including Rho GTPases, phosphatidylinositol 3-kinase (PI3K), extracellular signal-regulated kinase (ERK), p38 mitogen-activated protein kinase (p38 MAPK), Src kinase, Akt kinase or calcium ions were proposed as essential in cell electrotaxis [22–24]. However, the 'sensor' responsible for the initial detection of the presence of an applied EF still remains elusive.

In this study, we examined the influence of EF on migration of mouse bone marrow-derived cells and its potential role as a factor attracting mesenchymal stem cells to the wound site. We also addressed the question which factor is responsible for cathodal or anodal direction of cell movement. Finally, we analyzed the kinetics of electric field detection by cells.

2. Materials and methods

2.1. Cell isolation and culture

4- to 6-week-old C57Bl/6 mice were sacrificed by cervical dislocation and tibias and femurs were harvested immediately after animal euthanasia. Bone marrow adherent cells (BMACs) were isolated by flushing cavities of femurs and tibias with DMEM/F12 medium (Sigma-Aldrich). Cells were centrifuged, re-suspended in complete medium (DMEM/F12 with 10% FBS, Sigma-Aldrich; and 1% penicillin/streptomycin, P/S, Sigma-Aldrich) and seeded into a Primaria culture flask (BD Falcon) at a density of 3×10^5 nucleated cells/cm^2. The nonadherent cell population was removed after 72 h and the adherent layer was washed once with fresh medium. Cells were passaged with 0.25% trypsin/EDTA (Gibco, Life Technologies) when confluence of cells reached close to 90% and were typically diluted 1:2 at each passage. All procedures were performed in accordance with the approval of the Ethical Committee on Animal Testing at the Jagiellonian University (JU) in Krakow (approval number: 56/2009).

2.2. Electric field application

2 to 5 passage BMACs were exposed to EF at a strength of 50–300 mV/mm in the plexiglass apparatus described in detail by Korohoda et al. [25]. Briefly, EF was applied for 4 h through Ag/AgCl reversible electrodes of 6 cm^2 immersed in saline-filled wells connected by agar bridges (2% agar in 0.5 n KCl, 8 cm long) to neighbouring wells, to which the observation chambers were attached. The observation chambers were made of cover glasses measuring 60 × 35 × 0.2 mm. The investigated cells were plated for 2 h onto one of the cover glasses at a density of 2×10^4 cells/cm^2 and incubated in DMEM/F12 supplemented with 10% FBS in a humidified atmosphere with 5% CO_2 at 37 °C. Then the chamber was mounted with silicone grease in the plexiglass apparatus.

2.3. Signalling pathway analysis

In some experiments BMACs were pre-incubated for 1 h with 50 μM NSC23766 (Rac1 inhibitor, Calbiochem), 50 μM ZCL278 (Cdc42 inhibitor III, Calbiochem), 30 μM Rhosin (Rho inhibitor, Calbiochem) or for 30 min with 10 μMY-27632 (ROCK inhibitor, Calbiochem), 100 μM CK-666 (Arp2/3 inhibitor, Sigma-Aldrich), 10 μM LY-294002 (PI3K inhibitor, Sigma-Aldrich), 50 μM U0126 (MEK1/2 inhibitor, Sigma-Aldrich), 5 or 20 μM DMPQ-2HCl (PDGFRβ inhibitor, Abcam), 20 μM PQ401 (IGF1R inhibitor, Abcam), 10 or 50 μM NSC668036 (Dishevelled inhibitor, Sigma-Aldrich), 10 μM AG1478 (EGFR inhibitor, Sigma-Aldrich), 5, 20 or 50 μM PD158780 (EGFR inhibitors, Abcam) in DMEM/F12 with 10% FBS. In all cases inhibitors were present in medium throughout the 4 h of experiment.

To investigate the role of Ca^{2+} in electrotaxis, intra- or extracellular calcium ions were eliminated in different approaches. The intracellular Ca^{2+} were complexed with cell-permeant chelator BAPTA-AM (Calbiochem). In these experiments cells were loaded by 30 min preincubation with 1 μM BAPTA-AM in DMEM/F12 supplemented with 0.5% BSA (Sigma-Aldrich). The extracellular calcium ions were eliminated either by changing experimental medium to serum-free and calcium-free DMEM/F12 supplemented with 1% P/S or by addition of 0.5 mM EGTA (Sigma-Aldrich) to calcium-free DMEM/F12 with 10% FBS. Ion influx through mechanosensitive channels was prevented by 30 min cell pre-incubation with 3 μM GsMTx-4 (Smartox) - the inhibitor of stretch-activated channels.

2.4. Cell movement analysis

The movement of BMACs was time-lapse recorded for 4 h at 5 min time intervals, both in isotropic conditions and in EFs. The tracks of individual cells were determined from the series of changes in cell centroid positions, pooled and analyzed as previously described [26]. The following parameters were estimated: (i) the displacement length (μm), i.e. the distance from the starting point directly to the cell's final position, (ii) the cell speed (μm/h), i.e. trajectory length/time of recording, (iii) the coefficient of movement efficiency (CME) corresponding to the ratio of cell displacement to cell trajectory length, (iv) average directional cosines γ; γ is defined as the directional angle between the *x*-axis (parallel to the field direction) and the vector AB. A and B are the first and subsequent positions of the cell, respectively. Trajectories of cells from no less than two independent isolations (number of cells >20) were taken for the estimation of statistical significance.

2.5. Cell shape analysis

The parameters characterizing cell morphology were calculated as described by Dunn and Brown [27]. The following parameters were estimated: (i) cell area (μm^2) and (ii) cell elongation, a measure of how much the shape must be compressed along its long axis to minimize its extension. The minimum elongation of zero is only achieved if the shape is a circle and increases without limit as the shape becomes more elongated.

2.6. Cell sorting

For cell sorting, BMACs between 2 and 5 passage were harvested by 0.25% trypsin-EDTA and re-suspended in sorting medium containing DMEM/F12 supplemented with 2% FBS and 2% P/S. For cell sorting based on CD45 expression, cells were additionally stained with 1.5 μg/10^{6}cells of rat-anti-CD45-FITC monoclonal antibody (BD Biosciences). Then cells were incubated for 30 min on ice in the dark and washed with DMEM/F12 containing 2% FBS. Next, cells were re-suspended in sorting medium, filtered through a 70 μm filter (BD Falcon) and sorted with FACSAria (Becton Dickinson). After separation, cells were seeded into Primaria flasks in complete medium (DMEM/F12

with 10% FBS and 1% P/S). $CD45^+$ cells were cultured with addition of 50% of conditioned medium obtained from the culture of $CD45^-$ cells ($CD45^-$ cells of confluency no <70% were cultured for 48 h, then medium was collected, centrifuged for 10 min at 3000 rpm to exclude cell debris and kept for further use in −20 °C).

2.7. In vitro differentiation assays

For adipogenic differentiation, sorted $CD45^-$ cells were seeded in 6-well plates and cultured in complete medium. Upon reaching confluence, adipogenic induction medium (DMEM with 1000 mg/L glucose, 10% FBS, 0.1 μM dexamethasone, 0.5 mM 3-isobutyl-1-methylxanthine, 5 μM bovine insulin and 1% P/S) was applied for 14 days. Cells were fixed in 3.7% formaldehyde and stained with Oil red O (all from Sigma-Aldrich) [28].

For osteogenic differentiation, sorted $CD45^-$ confluent cells were stimulated with osteogenic induction medium (DMEM with 1000 mg/L glucose, 10% FBS, 10 nM dexamethasone, 50 μg/mL 2-phospho-L-ascorbic acid and 5 mM glycerol 2-phosphate, 1% P/S) for 28 days and then stained with Alizarin Red S (all from Sigma-Aldrich) [29].

2.8. Immunofluorescent staining

Cells were seeded on cover glasses measuring 60 × 10 × 0.2 mm for 2 h. Then the electrotactic chamber was mounted and cells were stimulated for 2 h with EF of 0 or 300 mV/mm. Afterwards, cells were fixed with 3.7% formaldehyde in PBS at room temperature for 20 min and permeabilized with 0.01% Triton X-100 (Sigma) in PBS for 5 min. For CD11b staining, cells were seeded 24 h before fixation on standard cover slips (15 × 15 mm). After washing with PBS nonspecific binding sites were blocked with 3% (w/v) bovine serum albumin in PBS (Sigma-Aldrich) for 45 min. Cells were stained for 1 h with rat anti-CD11b (1:200; Abcam) or rabbit anti-EGFR monoclonal antibody (1:250, Abcam). After washing the following secondary antibodies were applied for 1 h: Alexa Fluor 488-conjugated anti-rat IgG (1:300 Invitrogen) or Alexa-488 conjugated goat anti-rabbit IgG (1:300 Invitrogen). Nuclei were visualized with 1 μg/mL Hoechst 33258 (Sigma-Aldrich) added to secondary antibody solution. The cover slips were covered with Dako fluorescence mounting medium (Dako GmbH).

2.9. Proteomic analysis

BMACs from the second passage were sorted based on CD45 antigen expression and seeded into a Primaria culture flask at a density of 1×10^6 cells/25 cm^2. After 24 h cells were washed 6 times with PBS, lysed in 600 μL of 4% SDS and 0.1 M DTT in Tris-HCl pH 7.6 and sonicated for 10 min (320 W, 30 s/30 s on/off) using BioruptorTM UCD-200 (Diagenode). Then samples (three biological replicates in each group) were incubated at 95 °C for 5 min, centrifuged at 16,000 xg for 15 min at 20 °C and prepared for Filter Aided Sample Preparation (FASP) for LC–MS/MS analysis based on procedures described by Wisniewski et al. [30]. Peptides were obtained from samples after subsequent digestion with LysC protease (fraction 1) followed by trypsin digestion (fraction 2). FASP peptides for each fraction were analyzed separately by mass spectrometry (MS) using an UltiMate 3000RS LC nanoSystem (Dionex) coupled with a Q-Exactive mass spectrometer (Thermo Fisher Scientific) with DPV-550 Digital PicoView nanospray source. Database searching of RAW files was performed in Proteome Discoverer 1.4 (Thermo Fisher Scientific). MASCOT 2.5.1 was used for database searching against the SwissProt database with Rodentia taxonomy restriction (release December 2015, 26379 sequences). The following criteria were adopted: a given differential protein was identified in at least two of three biological replicates within one group on the basis of two or more unique peptides and no peptide belonging to this protein was identified in the samples of the second group.

2.10. Kinetics of cell return

Cells were prepared for EF stimulation as described in 2.2. Migrating cells were recorded for 1 h at a time interval of 30 s. To detect the reaction of BMACs to changes in EF direction, cells were recorded for 30 min in EF and then (when all cells were polarized), the direction of the field was changed. For a quantitative description of cell reaction, the projections of new surface area of right and left sides of cells were measured with ImageJ software (National Institute of Health). The right and the left sides of cells were estimated as follows: cell surface projection was divided into 3 parts along with the x axis (Fig. 9D). The right side of the cell corresponded to the 1/3 fragment of the cell surface facing the cathode and, after field reversal, the anode. The left side corresponded to the opposite surface. The centre of the cell was excluded from the analysis. The difference in area of right or left sides between two positions of a cell at different times t_0 and t was calculated according to the formula [31]:

$$S = ((S_t - S_0))/S_0$$

where: S_t – surface area at time t, S_0 – surface area at time t_0, t_0–5 min before field reversal. Quantitative analysis was performed for 5 min before and 5 min after field reversal with a 30 s time interval. Visualization of cell surface projection changes was done with the Corel PaintShop Pro X6 software (Corel Corporation). Cell contours at the moment of field reversal and 1, 3 or 5 min later were merged. The zone of lamellipodium expansion was marked green, whereas the zone of cell retraction red.

2.11. Statistical analysis

Data are reported as mean ± standard error of the mean (SEM), with 'n' denoting the number of cells. Means were compared using Kruskal-Wallis test in group comparison. The Mann-Whitney *U* test for unpaired data was applied as appropriate. A value of $p < 0.05$ was considered statistically significant. Analysis was performed in Statistica 10 software (StatSoft).

3. Results

3.1. Mouse bone marrow adherent cells consist of two populations migrating in the electric field in opposite directions

Mouse bone marrow adherent cells migrated randomly in absence of an EF with an average migration speed of 30.0 ± 0.04 μm/h and an average directional cosine γ close to zero (−0.09 ± 0.07) (Fig. 1, Supplementary Movie A). After application of the 300 mV/mm EF, cell speed accelerated to 42.0 ± 3.0 μm/h and the cosine γ value changed slightly to the range specific for anodal migration (−0.20 ± 0.11, Fig. 1, Supplementary Movie B). However, analysis of movies and graphs presenting cell trajectories reveals two subpopulations of cells migrating in the EF in opposite directions (Fig. 1B). After the separation of trajectories, these populations migrated in a highly directed fashion: the first migrated toward the cathode with an average cosine γ of 0.84 ± 0.04 and the second to the anode with cosine γ of −0.90 ± 0.02 (Fig. 2A, Table 1). Moreover, the differences in morphology of cells migrating in opposite directions were striking. Cells migrating toward the cathode were relatively large (3052 ± 214 μm^2, Table 1), flattened, and after application of the EF, elongated perpendicular to the direction of the EF. On the other hand, anode-migrating cells were consistently smaller (734 ± 32 μm^2, Table 1) and more elongated (cell elongation before EF application was 1.76 ± 0.12 compared to 0.39 ± 0.04 for cathode migrating cells, Fig. 2B, Table 1). For the purposes of this paper we named the population of cells migrating cathodally C-BMAC (from *Cathode-Migrating Bone Marrow Adherent Cells*) and the population migrating toward the anode A-BMAC (from *Anode-Migrating Bone Marrow Adherent Cells*).

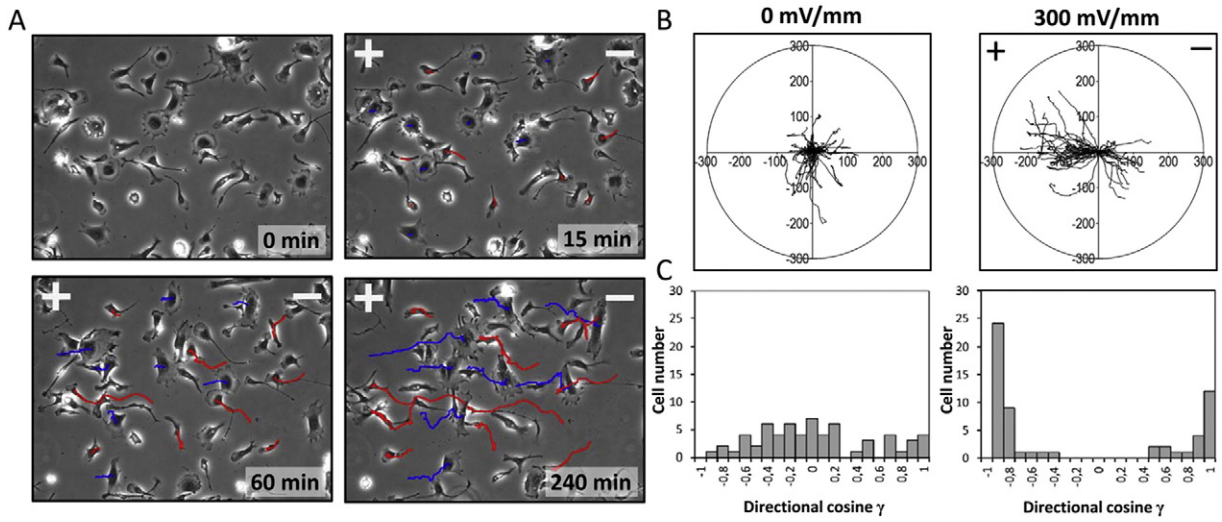

Fig. 1. Migration of BMACs in isotropic conditions and in electric field of 300 mV/mm. (A) Photographs of BMACs migrating in the EF of 300 mV/mm at indicated time points. Red lines – trajectories of cells migrating toward the anode (left), blue lines – trajectories of cell migrating toward the cathode (right), magnification 200×. (B) Diagrams presenting trajectories of BMAC cells migrating in the EF of 0 and 300 mV/mm for 4 h. Scale in μm, $n > 30$. (C) Histograms of directional cosine γ distribution in BMAC population for cells migrating in 0 and 300 mV/mm.

The electrotaxis C-BMAC was voltage-dependent and was evident already in EF as low as 50 mV/mm, since directionality of C-BMAC migration at 50 mV/mm was 0.46 ± 0.12 compared with −0.06 ± 0.09 for control cells (no EF). The increasing directionality of C-BMACs peaked in the EF of 300 mV/mm, with a cosine γ value of 0.84 ± 0.04 (Fig. 2C,D; solid line). The A-BMACs exhibited less directed migration at 50 mV/mm compared to C-BMACs with directional cosine value of −0.23 ± 0.09, however, the directionality of A-BMACs migration peaked at 200 mV/mm (cosine γ = −0.89 ± 0.02; Fig. 2C,D; dotted line). Given the 300 mV/mm EF was optimal for efficient electrotaxis of both cell populations, in further experiments we used EFs of this strength.

3.2. Mouse MSC migrated toward the cathode, whereas macrophages toward the anode

To identify and characterize C-BMACs and A-BMACs in the heterogenous population of bone marrow adherent cells, we had to develop an effective and efficient way of cell separation. The simplest method was to separate cells based on differences in their size (Fig. 3A). Indeed, this approach resulted in obtaining pure C-BMACs (larger cells, FSC^{high}) and A-BMACs (smaller, FSC^{low}) that retained reactivity in the EF of 300 mV/mm (Fig. 3B–E). However, this separation technique resulted in a high loss in cell number. Fortunately, cell sorting based on CD45 antigen expression enabled obtaining pure populations of C-BMACs

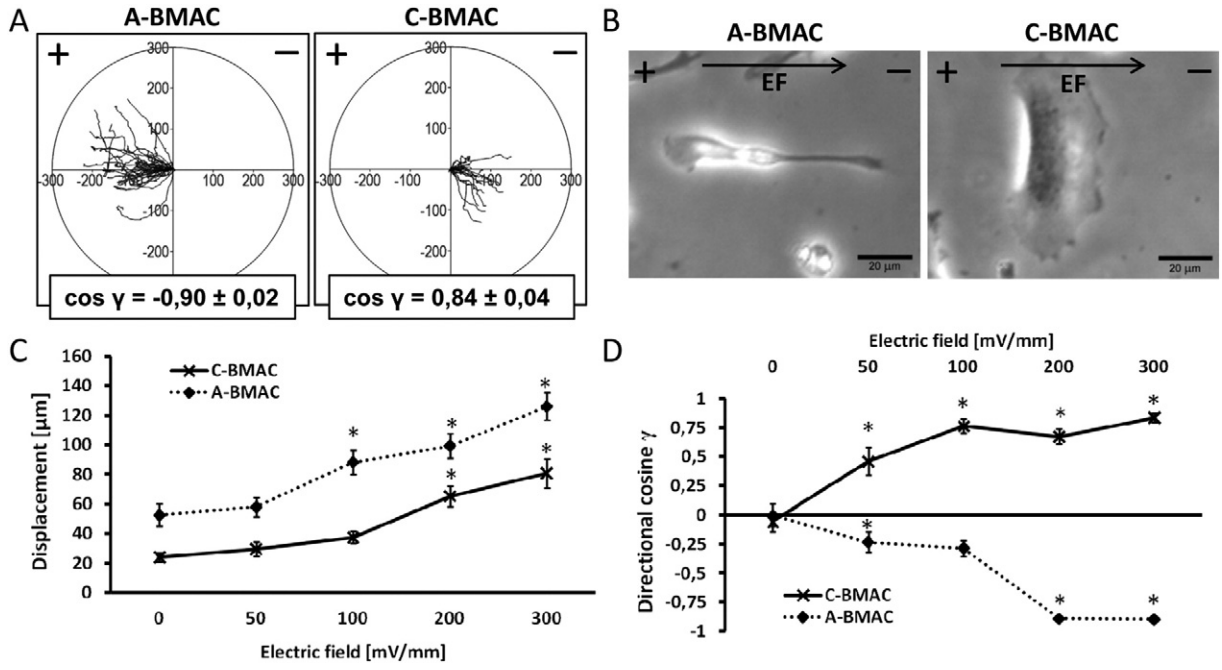

Fig. 2. Two populations of BMACs migrating in electric field in opposite directions. (A) Diagrams presenting the trajectories of anode-migrating (A-BMAC) and cathode-migrating (C-BMAC) bone marrow adherent cells. Scale in μm. Directional cosine γ presented as mean ± SEM. (B) Morphology of A-BMACs and C-BMACs migrating in the EF of 300 mV/mm for 4 h. Scale bar = 20 μm. Arrows indicate the direction of the EF. Analysis of cell displacement (C) or directionality (D) depending on the EF strength. Solid line – C-BMACs, dotted line – A-BMACs. Values presented as mean ± SEM, $n > 20$. * - indicate statistical significance compared to 0 mV/mm for $p < 0.05$, estimated with Kruskal-Wallis test.

Table 1
Parameters characterizing A-BMAC and C-BMAC migration in isotropic conditions and after the application of electric field.

Cell population	Cell area [μm²]	Cell elongation	Electric field [mV/mm]	Speed [μm/h]	Displacement [μm]	CDE	Directional cosine γ
A-BMAC	734 ± 32	1.76 ± 1.12	0	37,2 ± 3,0	52 ± 8	0,33 ± 0,04	-0.00 ± 0,1
			300	49,2 ± 3,6	126 ± 9*	0,65 ± 0.02*	-0.90 ± 0.02*
C-BMAC	3052 ± 214#	0.39 ± 0.12#	0	19,2 ± 1,8	25 ± 4	0,32 ± 0,04	-0.06 ± 0,09
			300	28,8 ± 1.8*	81 ± 10*	0,66 ± 0.04*	0,84 ± 0.04*

* Statistically significant vs. 0 mV/mm ($p < 0.05$), estimated with Mann-Whitney *U* test.
\# Statistically significant vs. A-BMACs ($p < 0.05$), estimated with Mann-Whitney *U* test.

(CD45⁻) and A-BMACs (CD45⁺) with high efficiency of cell number retrieval (Fig. 4, Supplementary Movies C, D). According to literature and our further results, we concluded that A-BMACs are bone marrow residing macrophages, as they adhered to the plastic and expressed both CD45 and CD11b antigens (Fig. 4B,D). At the same time, C-BMACs were also plastic-adherent but did not express either CD45 or CD11b and after appropriate stimulation were found to differentiate into osteoblasts or adipocytes (Fig. 4C). Taken together, we concluded that C-BMACs constitute a population of bone marrow mesenchymal stem cells.

3.3. Different signalling pathways are engaged in electrotaxis of C-BMACs and A-BMACs

Next, we investigated the signalling pathways that may lie at the core of differences in directional migration of C-BMCAs and A-BMACs. We examined all signalling pathways commonly ascribed to cell response to the EF. Pharmacological inhibition of Rho GTPases, i.e. Rac1, Cdc42 and RhoA had no effect on electrotaxis of C-BMACs. In all cases cell trajectories were present on the cathodal site of the diagrams and the directional cosine γ value after 4 h of EF stimulation did not change or only insignificantly decreased (up to 82% of control for Cdc42 inhibitor, Fig. 5B). A more distinct decrease in cell directionality was observed during the first hour of EF stimulation, suggesting that inhibition of Rho GTPases leads to delayed cell reaction to the electric field (Fig. 5A). Moreover, inhibition of Rho proteins caused a significant reduction of cell speed (up to 56% of control for Rac1, Fig. 5C).

Inhibition of Arp2/3, ROCK or PI3K had a more pronounced effect on C-BMAC directionality with the highest cosine γ decrease after LY294002 treatment (~70% of control, Fig. 5B). Once again, the strongest effect of the applied agents was observed during the first hour of cell electrotaxis with reduction of cell directionality up to 30% of control for LY294002 (Fig. 5A). Interesting, ROCK kinase inhibition led to a significant increase in C-BMAC migration speed in the EF (Fig. 5C). The activation of Erk1/2 kinase seemed to have no relation to directionality of C-BMAC movement, however inhibition of Erk1/2 activation resulted in 33% of cell speed reduction compared to control (Fig. 5A–C). Calcium ions did not appear to be essential for C-BMAC directed migration in EF, however they may be involved in cell reaction, especially at the early phase of cell response. After the first hour of EF stimulation, we observed reduced cell directionality, but not in a statistically significant way (44–59% of control) in serum-free medium, in serum-free medium without calcium ions or in complete medium after cell loading with 1 μM of BAPTA-AM (Fig. 6A). Intriguingly, 0.5 mM EGTA in medium with 10% FBS but without calcium had no effect on cell migration directionality after both 1 and 4 h in the EF (Fig. 6A,B). Regardless of the observed differences in cosine γ value, after 4 h of EF stimulation, C-BMACs migrated in a highly directional fashion with directional cosine γ no <60% of control and trajectories of cell movement were all gathered on the cathode facing side of the diagram (Figs. 5A–C, 6A–C, data not shown).

Anode-migrating cells were more sensitive to Rho GTPases inhibitors. We observed more cell trajectories concentrated around the middle of the diagram, however a significant portion of cells tended to migrate toward the anode (data not shown). The directional cosine γ was lowest for A-BMAC treated with NSC23766 Rac1 inhibitor and amounted to 55% of the control after 4 h of EF stimulation (Fig. 5E). The Rac1 inhibitor had the most pronounced effect on A-BMAC

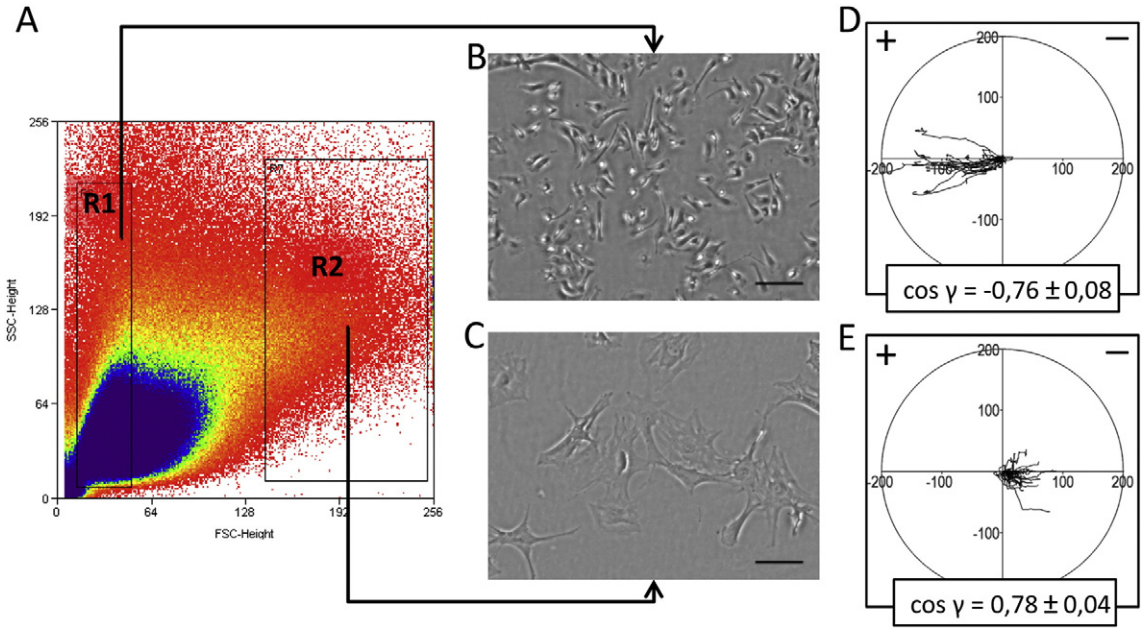

Fig. 3. BMACs separation based on differences in cell size. (A) Scheme of FACS sorting strategy. R1 – FSC^{low} cells corresponding to smaller cells, R2 - FSC^{high} cells corresponding to larger cells. Morphology of FSC^{low} (B) and FSC^{high} (C) cells after separation. Magnification 200×, Scale bar = 100 μm. Diagrams presenting trajectories of FSC^{low} (D) and FSC^{high} (E) cells migrating in EF of 300 mV/mm for 4 h. Directional cosine γ presented as mean ± SEM, $n > 20$. Scale in μm.

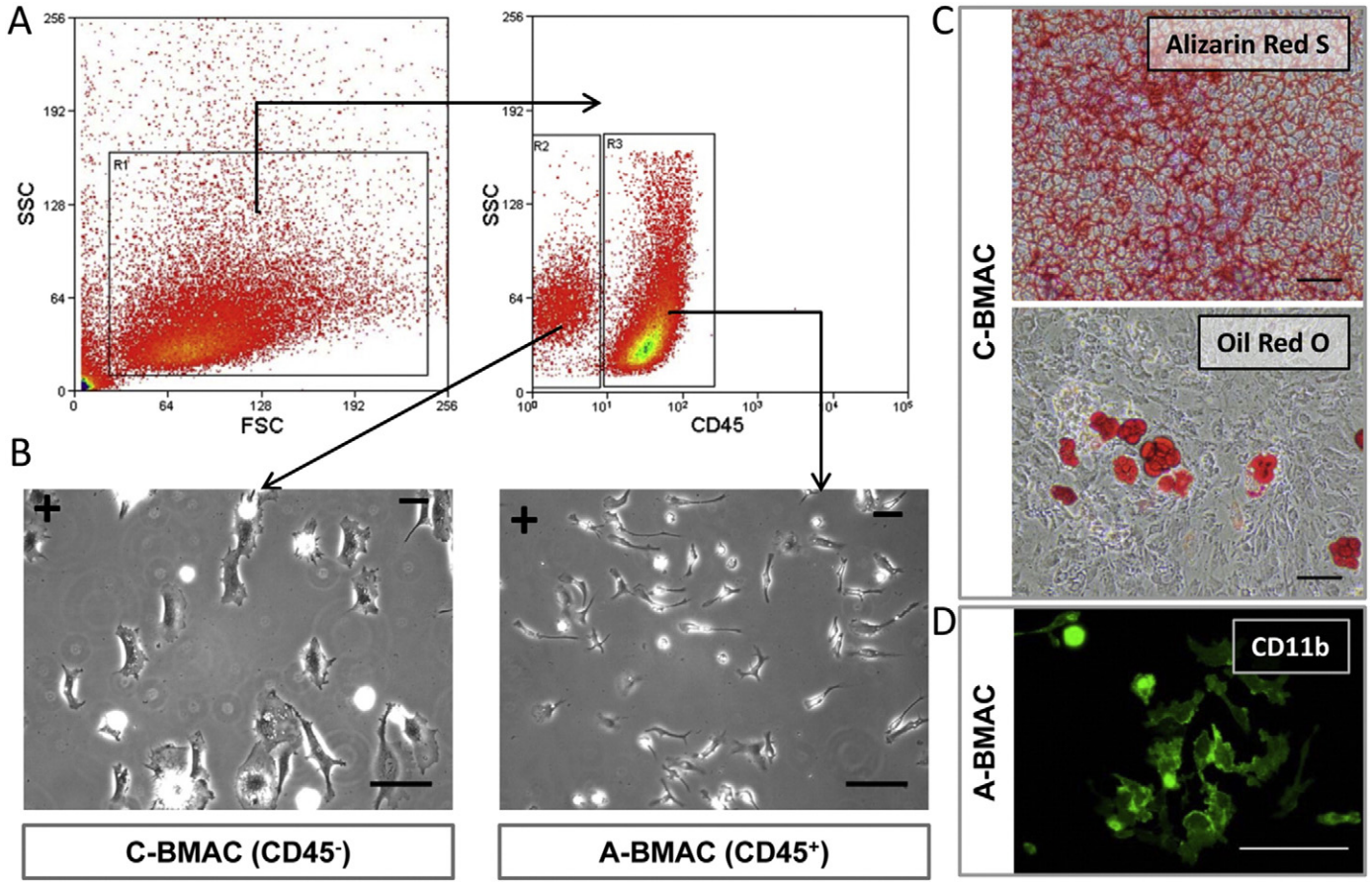

Fig. 4. Separation of BMACs based on CD45 antigen expression. (A) Strategy of BMAC separation with FACS. (B) Morphology of $CD45^{-}$ and $CD45^{+}$ cells migrating in EF of 300 mV/mm for 4 h. Magnification 200×. (C) Differentiation of pure population of C-BMACs to osteoblasts and adipocytes. Staining of the extracellular calcium deposit with Alizarin Red S in osteoblasts or fat droplets in adipocytes with Oil Red O. (D) Immunofluorescent staining of CD11b antigen, marker of macrophages in A-BMACs. Scale bar = 100 μm.

directionality during the first hour of treatment, with observed reduction of cosine γ value to 24% of control, suggesting the critical role of the cell lamellipodium during the first stage of A-BMAC electrotaxis (Fig. 5D). Moreover, all Rho GTPases inhibitors significantly decreased the speed of A-BMAC migration in the EF (Fig. 5F).

In spite of the supposed role of the lamellipodium in A-BMAC electrotaxis, inhibition of Arp2/3 complex essential for actin branching within lamellipodia had no effect on cell directionality, however, it significantly decreased the speed of cell migration (to 52% of control; Fig. 5D–F). At the same time, inhibition of ROCK kinase, involved in retraction of the trailing edge of a cell, not only did not decrease cell directionality, but significantly increased it with the most significant effect at the first hour of EF stimulation (212% of the control, Fig. 5D,E). Similar to C-BMACs, cell treatment with Y-27632 slightly increased the speed of A-BMACs, but not in a statistically significant manner (Fig. 5F). Application of inhibitors of PI3K and Mek1/2 kinases decreased A-BMAC directionality to 77% and 87%, respectively (Fig. 5E). In both conditions we also observed a significant reduction of cell speed to 37% of control for PI3K and 32% for Mek1/2 inhibition (Fig. 5F).

Analysis of calcium ion involvement in A-BMAC electrotaxis revealed that only simultaneous elimination of intra- and extracellular calcium ions led to complete inhibition of A-BMAC directionality (Fig. 6E). Moreover, we noticed a significant reduction of cell speed (49% of control) in this condition (1 μM BAPTA-AM, 0.5 mM EGTA, 10% FBS and DMEM/F12 w/o calcium, Fig. 6F).

In both cell populations, we did not observe any effect of mechanosensitive channel inhibition with specific peptide inhibitor GsMTx-4 on cell directionality (Fig. 6B,E). Although this may indicate that mechanosensitive ion channels are not involved in BMAC electrotaxis, the treatment with this peptide increased cell speed, especially for A-BMAC cells after 4 h of EF stimulation (194% of control, Fig. 6F).

3.4. Differential cell surface receptors are not crucial for C-BMACs electrotaxis

Another factor that could potentially explain the distinct reactions of both population of BMACs to EF was differential expression of chemotactic cell surface receptors. In order to select membrane receptors that might be involved in the detection of the electric field, we performed a shotgun LC–MS/MS analysis of protein content for each BMAC subpopulation (cathode- vs. anode-migrating cells). A comparison of protein sets obtained for both subpopulations revealed 2304 proteins exclusively identified in cathode-migrating cells, 322 proteins occurring solely in anode-migrating cells and 1119 proteins shared by both cell populations (Fig. 7A). Next we focused on an analysis of membrane proteins because they are directly exposed to the EF. According to the hypothesis stating that the redistribution of membrane receptors is a mechanism generating the directional migration in the EF, we selected 4 membrane receptors present exclusively on C-BMACs for further examination. It is particularly noteworthy that all of them, i.e. PDGFR, IGF1R, EGFR or Frizzled2, were described as engaged in electrotaxis of other cathode-migrating cells [17,19,32–37]. Once again we employed specific inhibitors to investigate the participation of these receptors in C-BMAC electrotaxis. For blocking of Fzd2 receptor we used NSC668036, a specific inhibitor of Dishevelled protein, as there is no

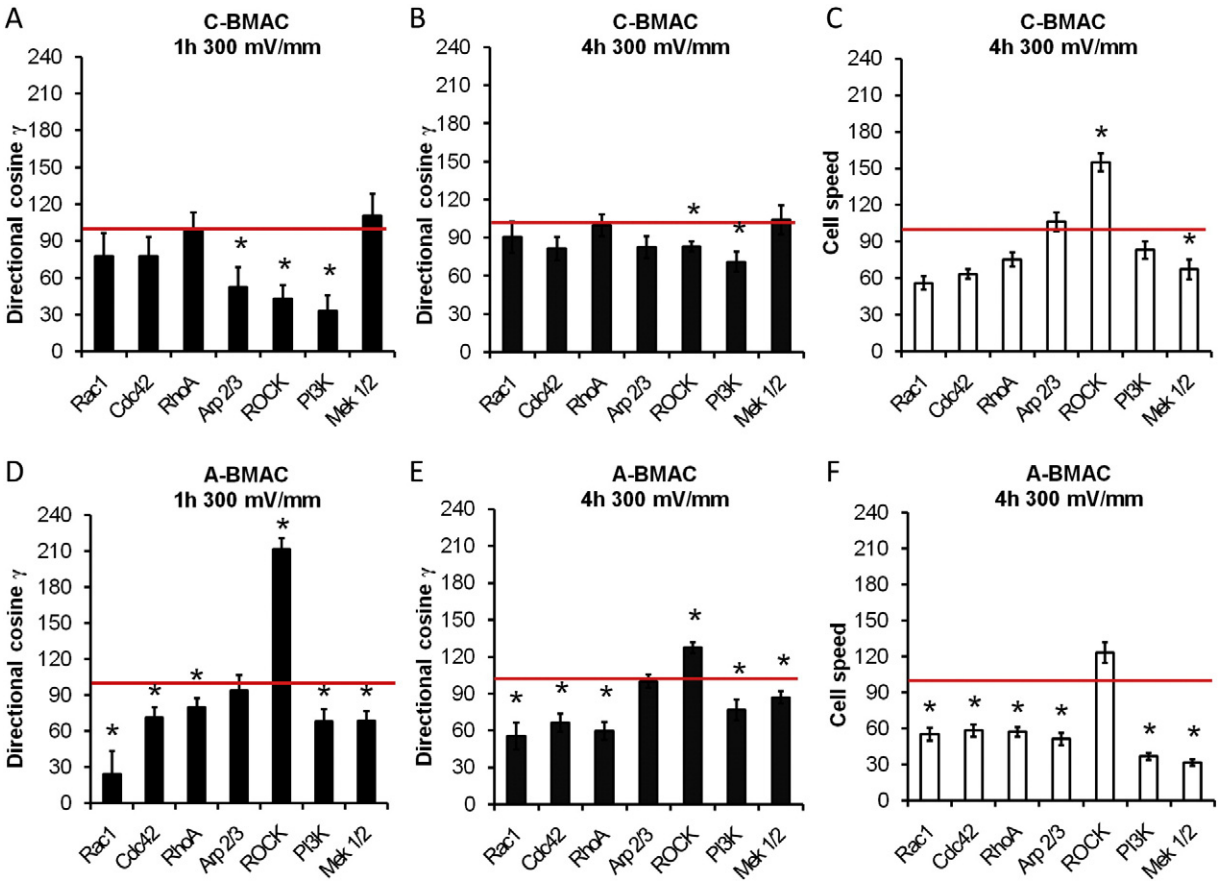

Fig. 5. Analysis of the contributions of different molecular pathways to C-BMAC and A-BMAC electrotaxis. Changes in cell directionality (A, B, D, E) and cell speed (C, F) after inhibition of indicated proteins. Cells were stimulated with electric field of 300 mV/mm for 1 (A, D) or 4 (B, C, E, F) hours in the presence of an appropriate inhibitor. Data presented as % of control (i.e. cells treated with 300 mV/mm without inhibitors) ± SEM. * - indicate statistical significance compared to control for $p < 0.05$ estimated with Kruskal-Wallis test.

compound dedicated to the inhibition of Frizzled 2 protein. We used several different concentrations of inhibitors with the lowest concentrations described by manufacturers as effective in cells and specific only for the proteins of interest. This approach was especially important in the case of the receptor tyrosine kinases (RTKs) because higher concentrations are known to inhibit other receptors from the RTKs family.

Our findings showed that neither PDGFRβ, IGF1R, nor Frizzled appeared to be critical for electrotaxis of C-BMACs. Only treatment with 5 μM of DMPQ-2HCl, PDGFRβ inhibitor, decreased cell directionality in a statistically significant way, however directional cosine γ still amounted to more than 60% of the control value and a further increase of the DMPQ-2HCl concentration had no effect on C-BMAC directionality (Fig. 7B). Moreover, inhibition of IGF1R with PQ401 significantly decreased the speed of C-BMAC migration in EF without influence on cell directionality (Fig. 7B,C).

A more detailed analysis was performed for EGFR, as this receptor is most frequently proposed as a "sensor" of an electric field, and EF-induced EGFR redistribution was presented in several types of cells. Although we used two different EGFR inhibitors, we demonstrated that inhibition of EGFR had no influence on directionality of C-BMAC cells (Fig. 8A,B). Only treatment with 50 μM PD158780 reduced cell speed to approximately one-half of the control without any influence on cell directionality (Fig. 8B). Surprisingly, we observed distinct accumulation of EGFR on the cathodal side of C-BMACs after 2 h of EF stimulation (Fig. 8C). In spite of the detected redistribution of the EGFR receptor, it did not seem to have any role in electrotaxis of C-BMACs. Also, we detected more EGFR at the edge of the cell lamellipodia in isotropic conditions.

3.5. Cell reaction to electric field reversal is highly dynamic.

Regarding the lack of complete abolishment of C-BMAC or A-BMAC directional migration in the case of all examined cellular pathways described to be engaged in both cell chemotaxis and electrotaxis, we analysed the dynamics of cell reaction in the EF. This approach determined the time frame of the mechanism that is responsible for the electrotactic reaction. We investigated the speed of cell return after EF reversal, with emphasis on the region where the cell reaction in EF is observed in the first place. If redistribution of growth factor receptors in the cell membrane was critical for EF detection, it would take minutes to hours for a cell to respond with repolarization due to reversal of EF direction.

Our results clearly showed that the cell reaction to EF reversal is highly dynamic, i.e. both A-BMACs and C-BMACs exhibited the first symptoms of repolarization as soon as 1 min after reversal of EF direction. Time needed for full repolarization differed between populations and equalled 5 and 10 min for A-BMACs and C-BMACs, respectively (data not shown).

The return of A-BMACs can be divided into two phases. In the first phase (time 1–3 min) cells retracted lamellipodia (at the left side of the cell – former anode, new cathode; red colour; Fig. 9B,C) and at this time the "new" leading edge of the cell was still elongated, resembling the trailing edge of a cell (Fig. 9A,B). In the next step (3–5 min), the new leading edge gradually expanded to the fully developed lamellipodium (right side, green colour; Fig. A,B, Supplementary Movie E). Quantitative analysis of cell surface changes confirmed that the cell retraction on the new cathode side took place within 30 s to

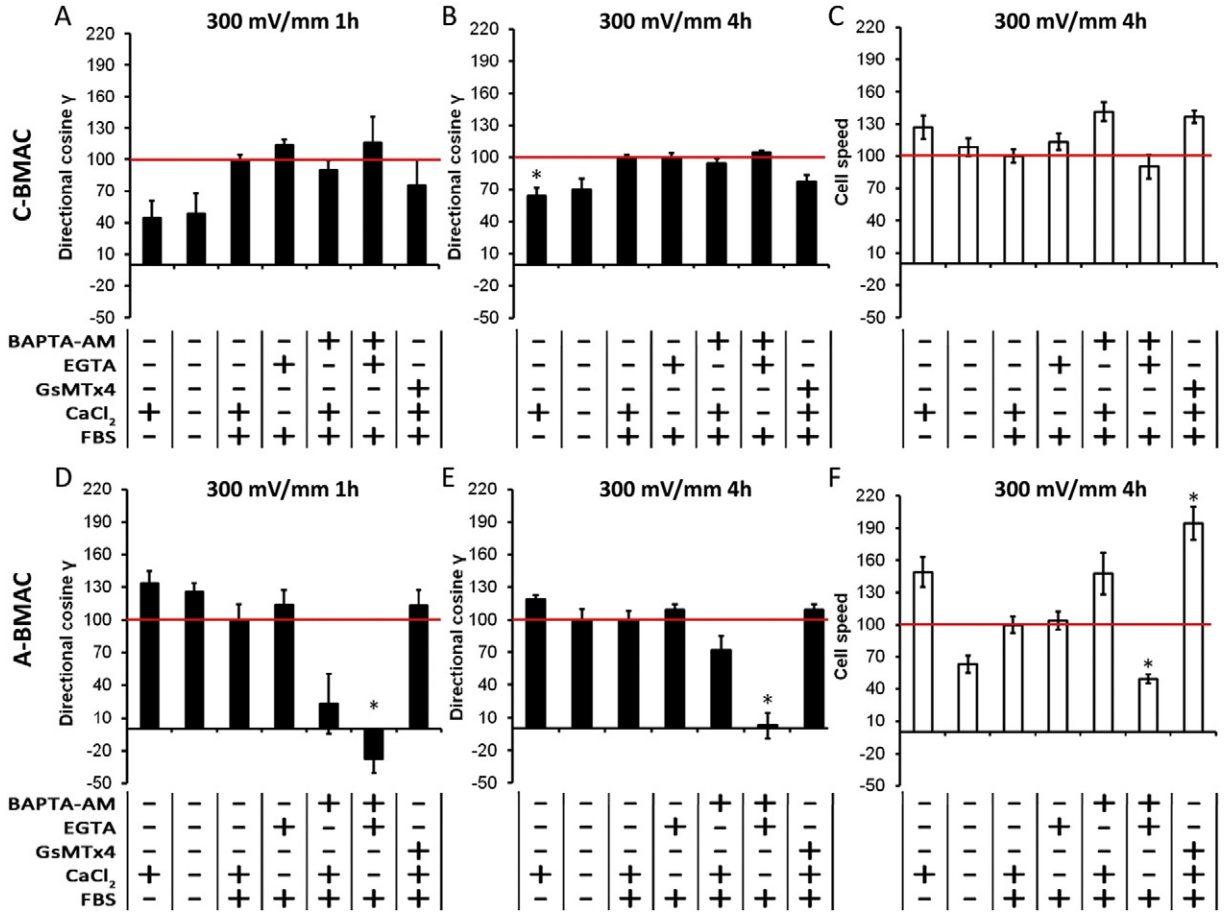

Fig. 6. Role of calcium ions in the electrotaxis of BMACs. The influence of calcium ion elimination on BMAC cell directionality (A, B, D, E) and cell speed (C, F). Cells were stimulated with EF of 300 mV/mm for 1 (A, D) or 4 (B, C, E, F) hours in DMEM F12 HAM medium with addition of 10% FBS, 1.05 mM $CaCl_2$, 3 μM GsMTx4 or 0.5 mM EGTA or after loading with 1 μM BAPTA-AM as indicated on charts. Data presented as % of control (i.e. cell treated with 300 mV/mm in standard culture medium with 10% FBS and 1.05 mM $CaCl_2$) ± SEM. * - indicate statistical significance compared to control for $p < 0.05$ estimated with Kruskal-Wallis test.

1 min after EF reversal for A-BMAC cells, whereas formation of a new lamellipodium only 3 min after EF reversal (Fig. 9C).

In contrast, the first changes at the C-BMACs surface occurred simultaneously in the front and in the rear of the cell and were observed as soon as 30 s after EF reversal (Fig. 10). Although there was a significant increase in the size of the new lamellipodium 5 min after EF reversal, it took the cell about 10 min to completely reverse polarization (Fig. 10C, data not shown). Interestingly, the new area of the lamellipodium was mostly produced not at the tip of the cell facing the new cathode, but at cell edges not exposed to electrodes, i.e. at the ends of cell along its long axis, perpendicular to the direction of EF (Fig. 10B, green colour, Supplementary Movie F).

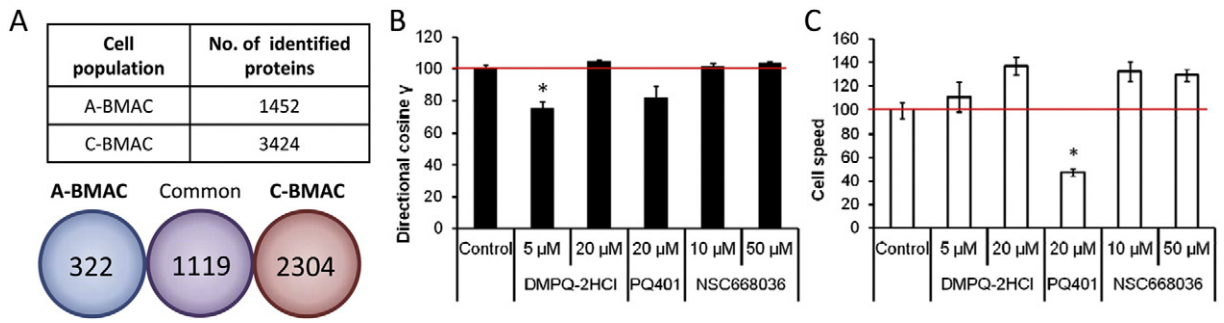

Fig. 7. Participation of selected protein receptors in the electrotaxis of C-BMACs. (A) Differential analysis of A-BMAC and C-BMAC proteoms. Influence of PDGFRβ (DMPQ-2HCl), IFG1R (PQ401) or Wnt pathway (NSC668036, Dishevelled inhibitor) inhibition on directionality (B) and speed (C) of C-BMAC electrotaxis. Cells were stimulated with EF of 300 mV/mm for 4 h. Data presented as % of control (i.e. cells treated with 300 mV/mm without inhibitors) ± SEM, $n > 20$. * - indicate statistical significance compared to control for $p < 0.05$ estimated with Kruskal-Wallis test.

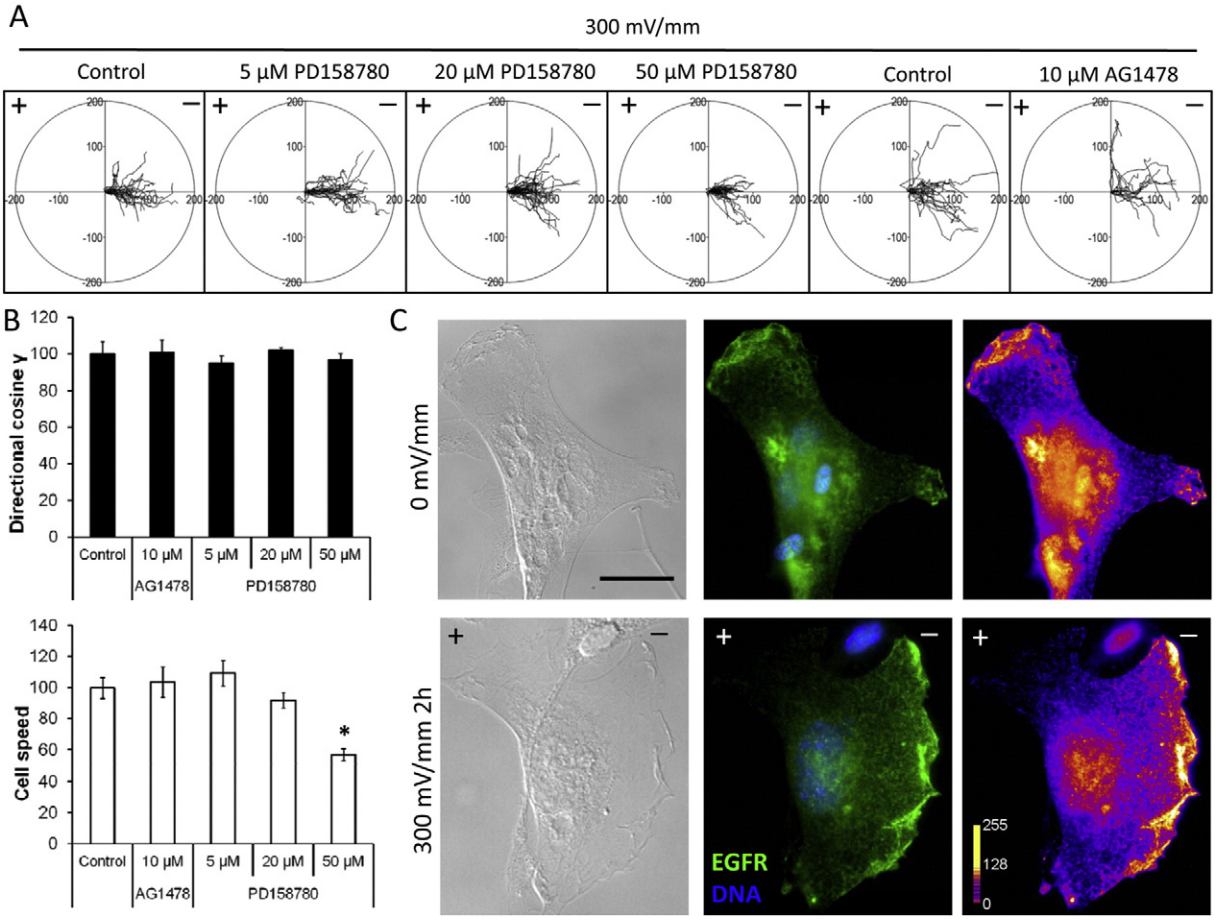

Fig. 8. The role of EGFR in C-BMAC electrotaxis. (A) Diagrams presenting C-BMAC cell trajectories in control conditions or after treatment with different concentrations of EGFR inhibitors. Scale in μm. (B) The influence of EGFR inhibition on C-BMAC directionality and speed in EF of 300 mV/mm. Cells were recorded for 4 h. Data presented as % of control (i.e. cell treated with 300 mV/mm without inhibitors) ± SEM, $n > 20$. * - indicate statistical significance compared to control for $p < 0.05$, estimated with Kruskal-Wallis test. (C) Immunofluorescent staining of C-BMACs for EGFR in isotropic conditions (0 mV/mm) or after 2 h in EF of 300 mV/mm. EGFR labelled with Alexa Fluor 488, nuclei counterstained with Hoechst 33258. Heat map of EGFR fluorescent intensity for better visualization of EGFR polarization in leading edge of a cell. Magnification 1000×, scale bar = 25 μm.

These findings emphasize that the mechanism lying at the base of detection of the EF by cells has to be immediate and dynamic because it is triggered within <1 min.

4. Discussion

The electric field (EF) is one of the first directional cues that appears in injured tissue, and is thus considered as a key factor responsible for cell recruitment to the wound site [8]. Moreover, there is much evidence suggesting that bone marrow mesenchymal stem cells may be mobilized from their natural niche to circulation and be engaged in skin wound healing [38–40]. In this study, we used an *in vitro* model to investigate whether bone marrow cells might be recruited by EF of physiological value to the wound site. We showed that BMACs consist of two cell populations migrating in EF in opposite directions, i.e. MSCs migrate toward the cathode, whereas macrophages toward the anode. Because of the high importance of MSC in regeneration processes, in the last few years several papers have considered electrotaxis of MSCs from different species and various tissue origin were published. Our results are in agreement with previous reports showing that human BM-MSCs and mouse adipose tissue-derived MSCs migrate toward the cathode in a similar range of EF [41,42]. This suggests that the direction of electrotaxis of specific types of cells is fixed and is not connected with tissue and species of origin. However, it is noteworthy that Zhao et al. [43] obtained contradictory results. They claimed that human BM-MSCs migrate mainly toward the anode and the percentages of anode and cathode migrating cells were 87% to 13%, respectively. Intriguingly, although they also observed two different bone marrow cell populations migrating in opposite directions in external EF, the investigated populations consisted only of MSCs because antigen analysis revealed no contamination with macrophages. Despite a general understanding of MSC homing, much work remains to be done to elucidate the molecular mechanisms responsible for each step [39]. The main hypothesis assumes that chemokine-chemokine receptor axes promote BM-MSCs mobilization and recruitment [39,40]. However, little is known about the mechanisms responsible for MSC guiding within a wound bed. Regarding the fact that the cathode is present at the centre of the wound in the case of skin injury, our results suggest that endogenous EFs may be an essential factor involved in MSCs recruitment to the wound site.

Similar conclusions considering the specificity of direction of cell electrotaxis may be drawn from results obtained on macrophages. As in our study, Orida et al. [44] observed that mouse peritoneal macrophages exhibit directional motility and protrusive activity toward the positive pole after application of EF. Moreover, human bone marrow macrophages were also shown to migrate toward the anode, as well as rabbit osteoclasts derived from macrophages [45,46]. This evidence strongly supports the hypothesis that macrophages represent the minor group of cells that tend to migrate toward the anode in EF. However, whether this is connected with their functions is unclear. We speculate that it is strongly desirable to keep macrophages at a close distance to a wound centre because of their indirect role in healing

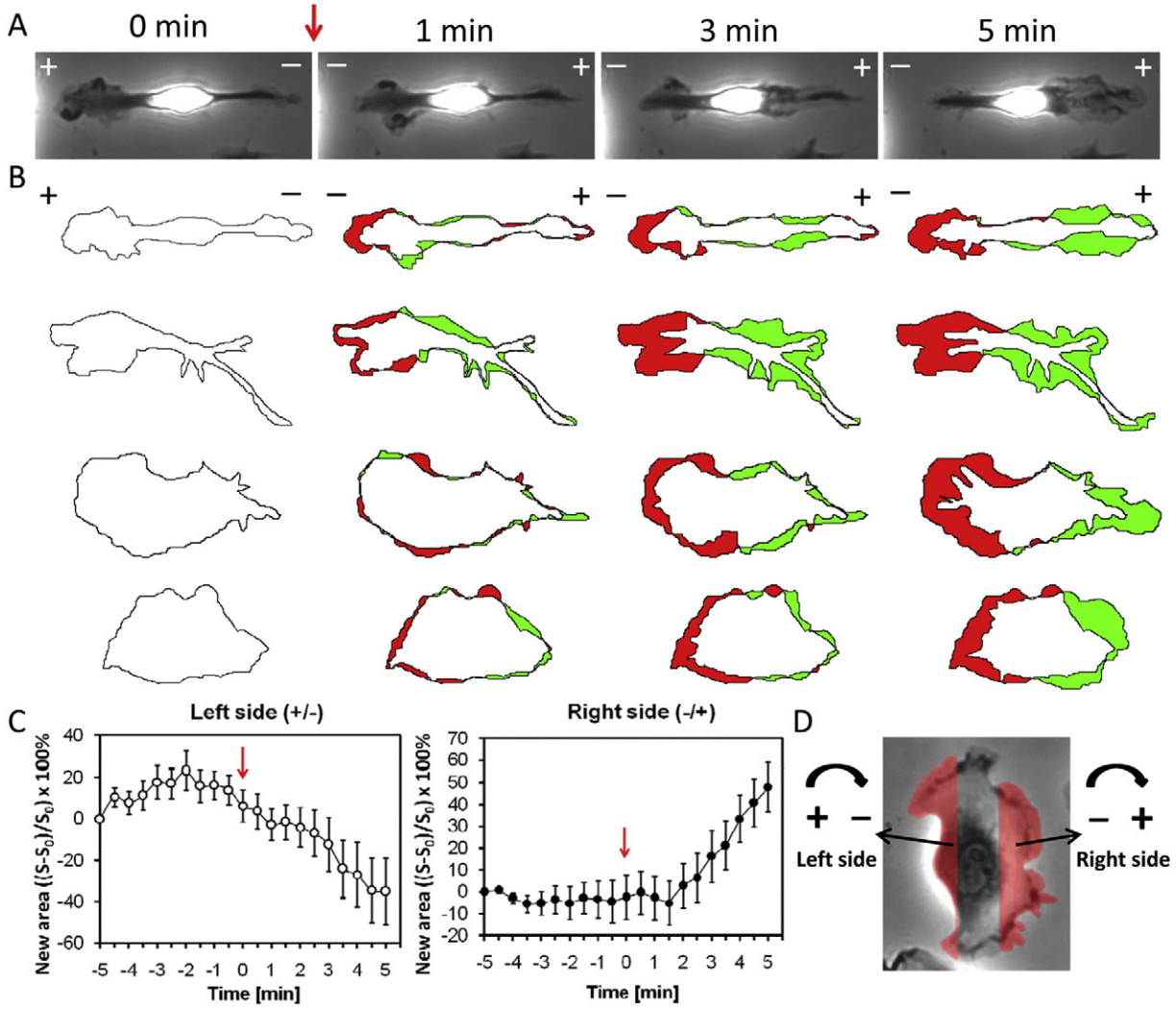

Fig. 9. Analysis of A-BMAC return after electric field reversal. (A) Phase contrast image sequence of A-BMAC turning after EF reversal (indicated with red arrow). (B) Analysis of changes in the cell surface projection between time of EF reversal and 1, 3 or 5 min after it. Red – retracted cell area, green – area of new lamellipodium formation. (C) Quantitative analysis of changes in the area of part of the cell facing new cathode (left side) or new anode (right side). Analysis performed 5 min before and 5 after the EF reversal with a time lapse of 30 s. Red arrow points moment of the EF reversal. Data presented as mean ± SEM, $n = 10$. (D) Scheme of cell division for quantitative analysis of cell return (details are given in Materials and Methods).

and functions they naturally perform, i.e. secretion of growth factors and ECM proteins [45].

We endeavoured to determine which factors are responsible for cathodal or anodal direction of cell movement in EF in our model of BMAC cells. It was suggested that the presetting of intracellular signalling networks may determine the direction of cell polarization, thus, cells may polarize in opposite directions to the same stimulus [47]. Although we used several inhibitors of various cellular pathways described to be involved in cell electrotaxis, we obtained only partial inhibition of cell directionality. Even when the directional cosine γ value decreased significantly in some cases, all cell trajectories were still oriented toward the same electrode as in control conditions (i.e. without inhibitor). Our findings indicate that Arp2/3, ROCK and PI3K take part in mesenchymal stem cells electrotaxis. However, because of only a slight decrease in cell directionality, which additionally was more evident in the first hour of EF stimulation, it is very likely that there are several overlapping intracellular pathways engaged in establishment and maintenance of cell polarity in EF. Thus, inhibition of only one of them delays the cell reaction to EF, but is not sufficient to completely abolish cell electrotaxis. Additionally, we must bear in mind that cellular pathways involved in directional cell movement are often responsible for cell motility itself. For this reason, analysis of signalling pathways is complicated, as the inhibition of electrotaxis at the same time often affects cell migration.

For macrophage electrotaxis, Rho GTPases, PI3K and MEK1/2 seem to be involved in the directional cell response but their inhibition only decreased cell directionality. Interestingly, simultaneous elimination of intra- and extracellular calcium ions completely abrogated macrophage electrotaxis. Calcium is a second messenger well known to be involved in the regulation of cell guiding and movement [48]. The hypothesis concerning the role of calcium ions in electrotaxis assumes that EF stimulates the influx of extracellular Ca^{2+} through membrane channels or/and the release of Ca^{2+} from intracellular stores and thus cell polarization induced by gradients of intracellular Ca^{2+} concentration [49]. However, based on the type of the investigated cells it was shown that electrotaxis is Ca^{2+}-dependent (e.g. for human and mouse keratinocytes or embryonic fibroblasts) or Ca^{2+}-independent (NIH 3T3) [24,50–52]. As calcium ions elimination affected electrotaxis of macrophages, but not MSCs, it seems likely that in our model Ca^{2+} engagement is also cell type-specific. Moreover, our results (demonstrating Ca^{2+}-dependent electrotaxis) are in agreement with the observation that Ca^{2+} play essential role in the maintenance of polarization of macrophages [53].

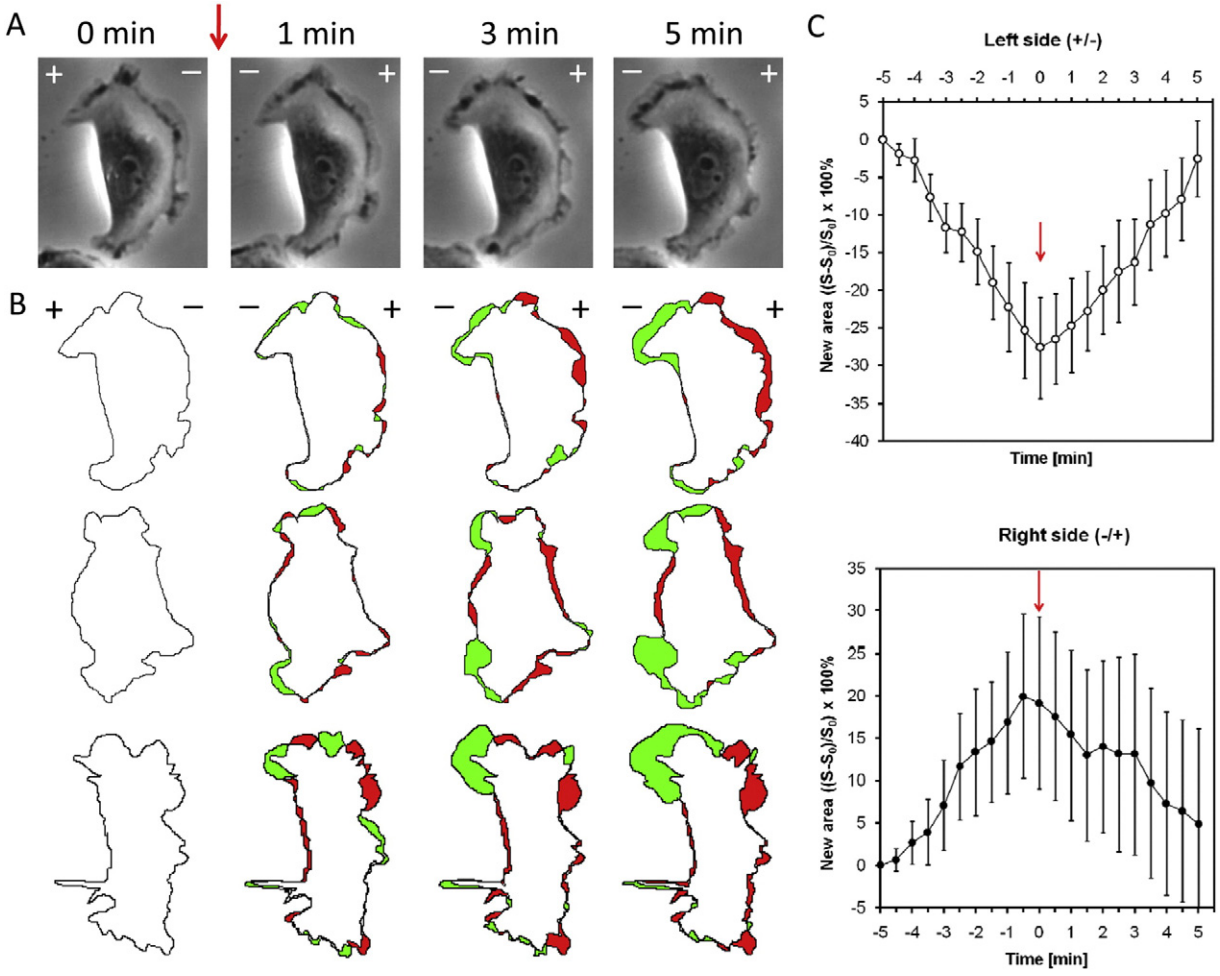

Fig. 10. Analysis of C-BMAC return after electric field reversal. (A) Phase contrast image sequence of C-BMAC turning after EF reversal (indicated with red arrow). (B) Analysis of changes in the cell surface projection between time of EF field reversal and 1, 3 or 5 min afterwards. Red – retracted cell area, green – area of new lamellipodium formation. (C) Quantitative analysis of changes in the area of part of the cell facing the new cathode (left side) or new anode (right side). Analysis performed 5 min before and 5 after EF reversal with a time lapse of 30 s. Red arrow points to moment of EF reversal. Data presented as mean ± SEM, $n = 10$.

The fact that EGTA and BAPTA-AM applied alone did not influence cell directionality complicates the mechanism of Ca^{2+} engagement. We suppose that there are overlapping pathways involving intra- and extracellular Ca^{2+} flux in macrophage electrotaxis, and after inhibition of only one of them, the second one is sufficient to support the cell reaction to EF. GsMTx-4 treatment ruled out some mechanosensitive ion channels as involved in electrotaxis, however, it is possible that other calcium channels may take part in this process. Nevertheless, further investigations are needed to resolve the exact mechanism of Ca^{2+} action.

Altogether, because we only observed a partial decrease in directionality of cell movement after inhibition of various signalling pathways in all cases, we suggest that involvement of these pathways in electrotaxis of MSCs and macrophages is not the cause of differences in the direction of their movement in EF.

Consistent with these observations, we assumed that specific surface receptors present in the cell membrane may be responsible for differential reaction to EF [54]. Nevertheless, our results revealed that none of the investigated receptors expressed exclusively in MSCs, i.e. EGFR, IGF1R, FGFR2 and Fzd2, were essential for detection of EF by these cells. Interestingly, similar to others [17,19], we observed accumulation of EGFR at the cathodal side of the cell. However, receptor redistribution might be a secondary event in cell electrotaxis, i.e. the result, not the cause of directional cell migration. Because the redistribution of cell membrane proteins often takes place when cells polarize even in the absence of external electric fields, a trend that was also observable in MSCs (Fig. 8C) [55].

The analysis of cell return after reversal of EF direction helped to establish the time frame of initial cell reaction to EF. As cells started to repolarize in the first 30 s after EF reversal, the detection of EF by cells has to be a very rapid and dynamic phenomenon. Electrophoretic/electroosmotic redistribution of charged membrane components seem not to be quick enough to result in a visible directional reaction in <1 min. Receptor migration requires many minutes for significant displacement to occur and the fastest experimentally observed accumulation of membrane receptors takes place within 5–10 min after EF application [11,19]. Similar conclusions were presented in our previous paper [25] where we had shown that in *Amoeba proteus* the initial response is visible in <1 s after electric field reversal, which is too rapid for the proposed electrophoretic/electroosmotic lateral redistribution of membrane receptors. Potential mechanisms matching the time frame of the events observed in our work include ion channel opening or the generation of a mechanic force on mechanosensitive membrane elements [49,56,57]. Our experiments with GsMTx-4 excluded mechanosensitive ion channels as a potential EF 'sensor' in MSCs and macrophages. These results do not support the hypothesis that EF-induced dragging of charged domains of mechanosensitive ion channels leads to their opening and ion influx. However, further studies are needed to determine whether other physical mechanisms, such as

generation of tension on membrane proteins connected with actin cytoskeleton, may be engaged [56].

In conclusion, our results suggest that the physiological direct current electric field may act as one of the factors in positioning MSCs within a wound bed and keeping macrophages at a close distance to the wound. The opposite direction of MSC and macrophage movement in the electric field did not result from utilizing different signalling or redistribution of cell surface receptors. Finally, we present evidence that the initial response to EF is very fast, suggesting the involvement of ionic or physical mechanisms.

Supplementary data to this article can be found online at doi:10.1016/j.bbamcr.2016.11.011.

Funding sources

This work was supported by the European Regional Development Fund within the Operational Programme Innovative Economy (POIG 01.02-00-109/99 "Innovative methods of stem cell application in medicine") and by a grant from the National Science Centre 2012/07/B/NZ3/02909, Poland. Faculty of Biochemistry, Biophysics and Biotechnology of Jagiellonian University is a partner of the Leading National Research Centre (KNOW) supported by the Ministry of Science and Higher Education. The mass spectrometric measurements were performed using a Q-Exactive spectrometer purchased by the European Regional Development Fund in the framework of the Polish Innovation Economy Operational Program (contract No. POIG.02.01.00-12-167/08, project Malopolska Centre of Biotechnology).

Transparency Document

The Transparency document, associated with this article can be found, in online version.

Acknowledgements

The authors would like to thank their co-workers Dr. Ewa Zuba-Surma and Urszula Jankowska. We also would like to show our gratitude to Professor Wlodzimierz Korohoda from the Department of Cell Biology, Faculty of Biochemistry, Biophysics and Biotechnology, Jagiellonian University, who introduced us to the theory and methodology of our work.

References

[1] G.C. Gurtner, S. Werner, Y. Barrandon, M.T. Longaker, Wound repair and regeneration, Nature 453 (2008) 314–321, http://dx.doi.org/10.1038/nature07039.
[2] W. Deng, Q. Han, L. Liao, C. Li, W. Ge, Z. Zhao, S. You, H. Deng, F. Murad, R.C.H. Zhao, Engrafted bone marrow-derived Flk-1$^+$ mesenchymal stem cells regenerate skin tissue, Tissue Eng. 11 (2005) 110–119, http://dx.doi.org/10.1089/ten.2005.11.110.
[3] L. Chen, E.E. Tredget, P.Y.G. Wu, Y. Wu, Paracrine factors of mesenchymal stem cells recruit macrophages and endothelial lineage cells and enhance wound healing, PLoS One 3 (2008), e1886http://dx.doi.org/10.1371/journal.pone.0001886.
[4] Y. Wu, L. Chen, P.G. Scott, E.E. Tredget, Mesenchymal stem cells enhance wound healing through differentiation and angiogenesis, Stem Cells 25 (2007) 2648–2659, http://dx.doi.org/10.1634/stemcells.2007-0226.
[5] S. Aoki, S. Toda, T. Ando, H. Sugihara, Bone marrow stromal cells, preadipocytes, and dermal fibroblasts promote epidermal regeneration in their distinctive fashions, Mol. Biol. Cell 15 (2004) 4647–4657, http://dx.doi.org/10.1091/mbc.E04-01-0038.
[6] M. Dominici, K. Le Blanc, I. Mueller, I. Slaper-Cortenbach, F. Marini, D. Krause, R. Deans, A. Keating, D. Prockop, E. Horwitz, Minimal criteria for defining multipotent mesenchymal stromal cells. The international society for cellular therapy position statement, Cytotherapy 8 (2006) 315–317, http://dx.doi.org/10.1080/14653240600855905.
[7] J.E. Bear, J.M. Haugh, Directed migration of mesenchymal cells: where signaling and the cytoskeleton meet, Curr. Opin. Cell Biol. 30 (2014) 74–82, http://dx.doi.org/10.1016/j.ceb.2014.06.005.
[8] C.D. McCaig, A.M. Rajnicek, B. Song, M. Zhao, Controlling cell behavior electrically: current views and future potential, Physiol. Rev. 85 (2005) 943–978, http://dx.doi.org/10.1152/physrev.00020.2004.
[9] R. Nuccitelli, P. Nuccitelli, S. Ramlatchan, R. Sanger, P.J.S. Smith, Imaging the electric field associated with mouse and human skin wounds, Wound Repair Regen. 16 (2008) 432–441, http://dx.doi.org/10.1111/j.1524-475X.2008.00389.x.
[10] R. Nuccitelli, P. Nuccitelli, C. Li, S. Narsing, D.M. Pariser, K. Lui, The electric field near human skin wounds declines with age and provides a noninvasive indicator of wound healing, Wound Repair Regen. 19 (2011) 645–655, http://dx.doi.org/10.1111/j.1524-475X.2011.00723.x.
[11] L.F. Jaffe, Electrophoresis along cell membranes, Nature 265 (1977) 600–602 (http://www.ncbi.nlm.nih.gov/pubmed/859558 (accessed January 12, 2016).
[12] M. Poo, J.W. Lam, N. Orida, A.W. Chao, Electrophoresis and diffusion in the plane of the cell membrane, Biophys. J. 26 (1979) 1–21, http://dx.doi.org/10.1016/S0006-3495(79)85231-5.
[13] S. McLaughlin, M.M. Poo, The role of electro-osmosis in the electric-field-induced movement of charged macromolecules on the surfaces of cells, Biophys. J. 34 (1981) 85–93, http://dx.doi.org/10.1016/S0006-3495(81)84838-2.
[14] L. Li, Y.H. El-Hayek, B. Liu, Y. Chen, E. Gomez, X. Wu, K. Ning, L. Li, N. Chang, L. Zhang, Z. Wang, X. Hu, Q. Wan, Direct-current electrical field guides neuronal stem/progenitor cell migration, Stem Cells 26 (2008) 2193–2200, http://dx.doi.org/10.1634/stemcells.2007-1022.
[15] M. Poo, K.R. Robinson, Electrophoresis of concanavalin A receptors along embryonic muscle cell membrane, Nature 265 (1977) 602–605 (http://www.ncbi.nlm.nih.gov/pubmed/859559 (accessed January 12, 2016).
[16] N. Ozkucur, S. Perike, P. Sharma, R.H.W. Funk, Persistent directional cell migration requires ion transport proteins as direction sensors and membrane potential differences in order to maintain directedness, BMC Cell Biol. 12 (2011) 4, http://dx.doi.org/10.1186/1471-2121-12-4.
[17] M. Zhao, J. Pu, J.V. Forrester, C.D. McCaig, Membrane lipids, EGF receptors, and intracellular signals colocalize and are polarized in epithelial cells moving directionally in a physiological electric field, FASEB J. 16 (2002) 857–859, http://dx.doi.org/10.1096/fj.01-0811fje.
[18] N. Orida, M.M. Poo, Electrophoretic movement and localisation of acetylcholine receptors in the embryonic muscle cell membrane, Nature 275 (1978) 31–35 (http://www.ncbi.nlm.nih.gov/pubmed/683340 (accessed December 29, 2015).
[19] K.S. Fang, E. Ionides, G. Oster, R. Nuccitelli, R.R. Isseroff, Epidermal growth factor receptor relocalization and kinase activity are necessary for directional migration of keratinocytes in DC electric fields, J. Cell Sci. 112 (Pt 1) (1999) 1967–1978 (http://www.ncbi.nlm.nih.gov/pubmed/10341215).
[20] C.E. Pullar, B.S. Baier, Y. Kariya, A.J. Russell, B.A.J. Horst, M.P. Marinkovich, R.R. Isseroff, beta4 integrin and epidermal growth factor coordinately regulate electric field-mediated directional migration via Rac1, Mol. Biol. Cell 17 (2006) 4925–4935, http://dx.doi.org/10.1091/mbc.E06–05-0433.
[21] C.-W. Huang, J.-Y. Cheng, M.-H. Yen, T.-H. Young, Electrotaxis of lung cancer cells in a multiple-electric-field chip, Biosens. Bioelectron. 24 (2009) 3510–3516, http://dx.doi.org/10.1016/j.bios.2009.05.001.
[22] a. M. Rajnicek, Temporally and spatially coordinated roles for Rho, Rac, Cdc42 and their effectors in growth cone guidance by a physiological electric field, J. Cell Sci. 119 (2006) 1723–1735, http://dx.doi.org/10.1242/jcs.02896.
[23] M. Zhao, B. Song, J. Pu, T. Wada, B. Reid, G. Tai, F. Wang, A. Guo, P. Walczysko, Y. Gu, T. Sasaki, A. Suzuki, J.V. Forrester, H.R. Bourne, P.N. Devreotes, C.D. McCaig, J.M. Penninger, Electrical signals control wound healing through phosphatidylinositol-3-OH kinase-γ and PTEN, Nature 442 (2006) 457–460, http://dx.doi.org/10.1038/nature04925.
[24] D.R. Trollinger, R. Rivkah Isseroff, R. Nuccitelli, Calcium channel blockers inhibit galvanotaxis in human keratinocytes, J. Cell. Physiol. 193 (2002) 1–9, http://dx.doi.org/10.1002/jcp.10144.
[25] W. Korohoda, M. Mycielska, E. Janda, Z. Madeja, Immediate and long-term galvanotactic responses of *Amoeba proteus* to dc electric fields, Cell Motil. Cytoskeleton 45 (2000) 10–26, http://dx.doi.org/10.1002/(SICI)1097-0169(200001)45:1<10::AID-CM2>3.0.CO;2-T.
[26] Z. Madeja, I. Szymkiewicz, A. Zaczek, J. Sroka, K. Miekus, W. Korohoda, Contact-activated migration of melanoma B16 and sarcoma XC cells, Biochem. Cell Biol. 79 (2001) 425–440 (http://www.ncbi.nlm.nih.gov/pubmed/11527212 (accessed August 16, 2016).
[27] G.A. Dunn, A.F. Brown, Alignment of fibroblasts on grooved surfaces described by a simple geometric transformation, J. Cell Sci. 83 (1986) 313–340 (http://www.ncbi.nlm.nih.gov/pubmed/3805145 (accessed February 11, 2016).
[28] M.A. Scott, V.T. Nguyen, B. Levi, A.W. James, Current methods of adipogenic differentiation of mesenchymal stem cells, Stem Cells Dev. 20 (2011) 1793–1804, http://dx.doi.org/10.1089/scd.2011.0040.
[29] J. Wang, B. Wang, Y. Li, D. Wang, E. Lingling, Y. Bai, H. Liu, High glucose inhibits osteogenic differentiation through the BMP signaling pathway in bone mesenchymal stem cells in mice, EXCLI J. 12 (2013) 584–597 (http://www.ncbi.nlm.nih.gov/pubmed/27103890 (accessed November 3, 2016).
[30] J.R. Wiśniewski, A. Zougman, N. Nagaraj, M. Mann, Universal sample preparation method for proteome analysis, Nat. Methods 6 (2009) 359–362, http://dx.doi.org/10.1038/nmeth.1322.
[31] A.K. Mittal, J. Bereiter-Hahn, Ionic control of locomotion and shape of epithelial cells: I. Role of calcium influx, Cell Motil. 5 (1985) 123–136 (http://www.ncbi.nlm.nih.gov/pubmed/3921256 (accessed July 20, 2016).
[32] X. Meng, M. Arocena, J. Penninger, F.H. Gage, M. Zhao, B. Song, PI3K mediated electrotaxis of embryonic and adult neural progenitor cells in the presence of growth factors, Exp. Neurol. 227 (2011) 210–217, http://dx.doi.org/10.1016/j.expneurol.2010.11.002.
[33] J. Banerjee, P. Das Ghatak, S. Roy, S. Khanna, E.K. Sequin, K. Bellman, B.C. Dickinson, P. Suri, V.V. Subramaniam, C.J. Chang, C.K. Sen, Improvement of human keratinocyte migration by a redox active bioelectric dressing, PLoS One 9 (2014) e89239, http://dx.doi.org/10.1371/journal.pone.0089239.
[34] C.-W. Huang, H.-Y. Chen, M.-H. Yen, J.J.W. Chen, T.-H. Young, J.-Y. Cheng, Gene expression of human lung cancer cell line CL1-5 in response to a direct current

electric field, PLoS One 6 (2011), e25928, http://dx.doi.org/10.1371/journal.pone.0025928.
[35] J. Liu, B. Zhu, G. Zhang, J. Wang, W. Tian, G. Ju, X. Wei, B. Song, Electric signals regulate directional migration of ventral midbrain derived dopaminergic neural progenitor cells via Wnt/GSK3β signaling, Exp. Neurol. 263 (2015) 113–121, http://dx.doi.org/10.1016/j.expneurol.2014.09.014.
[36] C. Wang, J. Dai, Z. Sun, C. Shi, H. Cao, X. Chen, S. Gu, Z. Li, W. Qian, X. Han, Targeted inhibition of disheveled PDZ domain via NSC668036 depresses fibrotic process, Exp. Cell Res. 331 (2015) 115–122, http://dx.doi.org/10.1016/j.yexcr.2014.10.023.
[37] M. Zhao, A. Dick, J.V. Forrester, C.D. McCaig, Electric field-directed cell motility involves up-regulated expression and asymmetric redistribution of the epidermal growth factor receptors and is enhanced by fibronectin and laminin, Mol. Biol. Cell 10 (1999) 1259–1276 (http://www.ncbi.nlm.nih.gov/pubmed/10198071 (accessed July 20, 2016).
[38] Y. Wu, R.C. Zhao, E.E. Tredget, Bone marrow derived stem/progenitor cells in cutaneous repair and regeneration, Stem Cells (2010), http://dx.doi.org/10.1002/stem.420 n/a–n/a.
[39] R.C. Rennert, M. Sorkin, R.K. Garg, G.C. Gurtner, Stem cell recruitment after injury: lessons for regenerative medicine, Regen. Med. 7 (2012) 833–850, http://dx.doi.org/10.2217/rme.12.82.
[40] A.M. Hocking, The role of chemokines in mesenchymal stem cell homing to wounds, Adv. Wound Care (4) (2015) 623–630, http://dx.doi.org/10.1089/wound.2014.0579.
[41] K.E. Hammerick, M.T. Longaker, F.B. Prinz, In vitro effects of direct current electric fields on adipose-derived stromal cells, Biochem. Biophys. Res. Commun. 397 (2010) 12–17, http://dx.doi.org/10.1016/j.bbrc.2010.05.003.
[42] T.A. Banks, P.S.B. Luckman, J.E. Frith, J.J. Cooper-White, Effects of electric fields on human mesenchymal stem cell behaviour and morphology using a novel multichannel device, Integr. Biol. (Camb) 7 (2015) 693–712, http://dx.doi.org/10.1039/c4ib00297k.
[43] Z. Zhao, C. Watt, A. Karystinou, A.J. Roelofs, C.D. McCaig, I.R. Gibson, C. De Bari, Directed migration of human bone marrow mesenchymal stem cells in a physiological direct current electric field, Eur. Cell. Mater. 22 (2011) 344–358 (http://www.ncbi.nlm.nih.gov/pubmed/22125259).
[44] N. Orida, J.D. Feldman, Directional protrusive pseudopodial activity and motility in macrophages induced by extracellular electric fields, Cell Motil. 2 (1982) 243–255 (http://www.ncbi.nlm.nih.gov/pubmed/6816471 (accessed December 29, 2015).
[45] J.I. Hoare, A.M. Rajnicek, C.D. McCaig, R.N. Barker, H.M. Wilson, Electric fields are novel determinants of human macrophage functions, J. Leukoc. Biol. (2015), http://dx.doi.org/10.1189/jlb.3A0815-390R.
[46] J. Ferrier, S.M. Ross, J. Kanehisa, J.E. Aubin, Osteoclasts and osteoblasts migrate in opposite directions in response to a constant electrical field, J. Cell. Physiol. 129 (1986) 283–288, http://dx.doi.org/10.1002/jcp.1041290303.
[47] Y. Sun, H. Do, J. Gao, R. Zhao, M. Zhao, A. Mogilner, Keratocyte fragments and cells utilize competing pathways to move in opposite directions in an electric field, Curr. Biol. 23 (2013) 569–574, http://dx.doi.org/10.1016/j.cub.2013.02.026.
[48] D.M. Graham, L. Huang, K.R. Robinson, M.A. Messerli, Epidermal keratinocyte polarity and motility require Ca^{2+} influx through TRPV1, J. Cell Sci. 126 (2013) 4602–4613, http://dx.doi.org/10.1242/jcs.122192.
[49] M.E. Mycielska, M.B.A. Djamgoz, Cellular mechanisms of direct-current electric field effects: galvanotaxis and metastatic disease, J. Cell Sci. 117 (2004) 1631–1639, http://dx.doi.org/10.1242/jcs.01125.
[50] E.K. Onuma, S.W. Hui, Electric field-directed cell shape changes, displacement, and cytoskeletal reorganization are calcium dependent, J. Cell Biol. 106 (1988) 2067–2075, http://dx.doi.org/10.1083/jcb.106.6.2067.
[51] K.S. Fang, B. Farboud, R. Nuccitelli, R.R. Isseroff, Migration of human keratinocytes in electric fields requires growth factors and extracellular calcium, J. Invest. Dermatol. 111 (1998) 751–756, http://dx.doi.org/10.1046/j.1523-1747.1998.00366.x.
[52] M.J. Brown, L.M. Loew, Electric field-directed fibroblast locomotion involves cell surface molecular reorganization and is calcium independent, J. Cell Biol. 127 (1994) 117–128 http://www.pubmedcentral.nih.gov/articlerender.fcgi?artid=2120190&tool=pmcentrez&rendertype=abstract (accessed January 12, 2016).
[53] J.H. Evans, J.J. Falke, Ca^{2+} influx is an essential component of the positive-feedback loop that maintains leading-edge structure and activity in macrophages, Proc. Natl. Acad. Sci. 104 (2007) 16176–16181, http://dx.doi.org/10.1073/pnas.0707719104.
[54] G.M. Allen, A. Mogilner, J.A. Theriot, Electrophoresis of cellular membrane components creates the directional cue guiding keratocyte galvanotaxis, Curr. Biol. 23 (2013) 560–568, http://dx.doi.org/10.1016/j.cub.2013.02.047.
[55] M.J. Brown, L.M. Loew, Graded fibronectin receptor aggregation in migrating cells, Cell Motil. Cytoskeleton 34 (1996) 185–193, http://dx.doi.org/10.1002/(SICI)1097-0169(1996)34:3<185::AID-CM2>3.0.CO;2-9.
[56] F.X. Hart, M. Laird, A. Riding, C.E. Pullar, Keratinocyte galvanotaxis in combined DC and AC electric fields supports an electromechanical transduction sensing mechanism, Bioelectromagnetics 34 (2013) 85–94, http://dx.doi.org/10.1002/bem.21748.
[57] K. Nakajima, K. Zhu, Y.-H. Sun, B. Hegyi, Q. Zeng, C.J. Murphy, J.V. Small, Y. Chen-Izu, Y. Izumiya, J.M. Penninger, M. Zhao, KCNJ15/Kir4.2 couples with polyamines to sense weak extracellular electric fields in galvanotaxis, Nat. Commun. 6 (2015) 8532, http://dx.doi.org/10.1038/ncomms9532.